The Astrophysical Journal, 878:33 (9pp), 2019 June 10 https://doi.org/10.3847/1538-4357/ab1be2

The Complex Nature of Magnetic Element Transport in the Quiet Sun: The Lévy-walk Character

F. Giannattasio[1], G. Consolini[2], F. Berrilli[3], and D. Del Moro[3]
[1] Istituto Nazionale di Geofisica e Vulcanologia, Via di Vigna Murata 605, I-00143 Roma, Italy
[2] INAF—Institute for Space Astrophysics and Planetology (IAPS), Via del Fosso del Cavaliere 100, I-00133 Roma, Italy
[3] Department of Physics, University of Rome Tor Vergata, Via della Ricerca Scientifica 1, I-00133 Roma, Italy
Received 2019 April 1; revised 2019 April 19; accepted 2019 April 22; published 2019 June 11

Abstract

The study of the dynamic properties of small-scale magnetic fields in the solar photosphere (magnetic elements, MEs) provides a fundamental tool to investigate some still unknown aspects of turbulent convection, and gain information on the spatial and temporal scales of evolution of the magnetic field in the quiet Sun. We track the MEs in a set of magnetogram long-time series acquired by the *Hinode* mission, and take advantage of a method based on entropy (the diffusion entropy analysis, DEA) to detect their dynamic regime, under the assumption that MEs are passively transported by the photospheric plasma flow. DEA has been proven to perform better than other standard techniques, and for the first time it is successfully used to provide the scaling properties of the displacement of MEs in the quiet Sun. The main results of this work, which represents an extension of the analysis presented in previous literature, can be summarized as two points: (i) MEs in the quiet Sun undergo a common dynamic turbulent regime independent of the local environment; (ii) the displacement of MEs exhibits a complex transport dynamics that is consistent with a Lévy walk.

Key words: Sun: granulation – Sun: photosphere

1. Introduction

The outer layers of the Sun are characterized by convective plasma motions that manifest in what is generally known as a *convective granulation pattern* at the solar photosphere. Due to the very high Rayleigh number, namely $Ra \sim 10^{19}$–10^{24}, these convective motions are expected to be in a highly turbulent state, showing a more complex spatiotemporal evolution than the simple Rayleigh–Bénard convection. Furthermore, the solar turbulent convection is also strongly affected by the magnetic field, which interacts with the solar plasma motions.

The interaction between turbulent convection and magnetic fields in the solar photosphere plays a fundamental role in feeding the upper atmosphere of energy and triggering a chain of phenomena relevant for space weather (see, e.g., Alfvén 1947; Parker 1957, 1988; Jefferies et al. 2006; Viticchié et al. 2006; De Pontieu et al. 2007; Tomczyk et al. 2007; Sobotka et al. 2014; Stangalini et al. 2014, 2015, 2017; Srivastava et al. 2017). This interaction is also responsible for the structuring of the solar photosphere at all scales, from granular (see, e.g., Berrilli et al. 1999, 2002, 2004; Consolini et al. 1999; Del Moro 2004; Nesis et al. 2006; Centeno et al. 2007; Del Moro et al. 2015) to mesogranular (see, e.g., November 1980; Roudier et al. 1998; Berrilli et al. 2005, 2013; Yelles Chaouche et al. 2011), and supergranular (see, e.g., Hart 1956; Simon & Leighton 1964; Berrilli et al. 2004, 2014; Del Moro et al. 2004; de Wijn et al. 2008; Orozco Suárez et al. 2012; Giannattasio et al. 2013, 2014a, 2014b, 2018; Stangalini 2014; Gošić et al. 2014, 2016). Nevertheless, many aspects of turbulent convection are still far from being completely unveiled. One reason is that the typical Rayleigh number (Ra) expected for solar convection is several orders of magnitude higher than those currently attainable in laboratory experiments ($Ra \sim 10^{17}$), so it is still impossible to test on Earth any theory explaining the onset of turbulent convection in the solar photosphere (see, e.g., Niemela et al. 2000; Hanasoge et al. 2012; He et al. 2012).

In light of this, three different approaches have been followed so far to gain insights into photospheric turbulent convection. (1) Magnetohydrodynamic (MHD) simulations (see, e.g., Nordlund & Stein 1997; Stein & Nordlund 1998, 2001; Cattaneo et al. 2003; Vögler et al. 2005; Rempel et al. 2009; Beeck et al. 2012; Danilovic et al. 2015) have reproduced the convective layer in a very detailed and realistic way, but in a limited range of spatial and temporal scales. In fact, due to the computational limitations of current computing power, it is still not possible to simulate all the scales involved, from subgranular to global. (2) The statistical analysis of plasma and/or magnetic features appearing in the photosphere on several spatial and temporal scales (see, e.g., Getling & Brandt 2002; Rast 2002; Getling 2006; Brandt & Getling 2008; Giannattasio et al. 2018) provided constraints on the appearance and evolution of these features via the correlation of coherent photospheric patterns in the quiet Sun, but gave little detail about the dynamic processes and laws at work. (3) Tracking magnetic elements (MEs) in magnetograms or bright features in *G*-band images (see, e.g., Wang 1988; Berger et al. 1998; Cadavid et al. 1998, 1999; Hagenaar et al. 1999; Lawrence et al. 2001; Sánchez Almeida et al. 2010; Abramenko et al. 2011; Manso Sainz et al. 2011; Lepreti et al. 2012; Giannattasio et al. 2013, 2014a, 2014b; Keys et al. 2014; Caroli et al. 2015; Del Moro et al. 2015; Yang et al. 2015a, 2015b; Roudier et al. 2016; Abramenko 2017, 2018; Agrawal et al. 2018), under the reasonable hypothesis that MEs in the quiet Sun are passively transported by the plasma flow (Petrovay & Szakaly 1993; Petrovay 1994; Giannattasio et al. 2013), it was possible to probe advection/diffusion processes in the photosphere and inspect the scales of organization of magnetic fields.

Approach (3) enabled noticeable progress toward fuller knowledge of the physical properties of the velocity fields

acting in the turbulent photosphere. In fact, transport in turbulent media, such as turbulent fluids and magnetohydrodynamic plasmas, is a complex phenomenon that displays scale-invariant and superdiffusive features. This is, for instance, the case for contaminant transport in turbulent media. In general, for scalar quantities that are passively advected in fully developed turbulent media, the diffusive motion of these quantities displays a character that significantly departs from the standard Brownian diffusion, which is characterized by the following motion law over time t:

$$\mathcal{L}_2(t) \sim t: \quad \mathcal{L}_2 = \langle r^2(t) \rangle, \tag{1}$$

with $\mathcal{L}_2$ being the mean-square displacement of passive quantities. In turbulent media the diffusive transport of a contaminant is strongly enhanced such that $\mathcal{L}_2$ acquires a faster dependence on time,

$$\mathcal{L}_2(t) \sim t^{\alpha}: \quad \alpha > 1, \tag{2}$$

where, generally, $\alpha \sim 3$ for turbulent fluid media. Furthermore, the α exponent is connected with the fractal dimension d_w of the transport path, $d_w = 2/\alpha$. We remark that there is also a link between the observed scaling properties of the displacement (such as the spectral properties of fluid motions) and the nature of the turbulence that drives the transport. In such a framework, the investigation of the motion of MEs in the quiet photosphere can provide information about the turbulent features of the solar convection, under the hypothesis that MEs are passively transported by the underlying flow. This assumption is well fulfilled only by the weak quiet Sun magnetic fields such as the internetwork fields, as their magnetic pressure is smaller than the plasma kinetic pressure (Petrovay 1994; Giannattasio et al. 2013)

In this work, for the first time we use an approach based on an entropic method to point out and characterize the complex nature of diffusion of MEs in the quiet Sun. In particular, we find evidence for a Lèvy-walk nature of diffusion, characterized by scaling features different from what is generally expected from the typical exponent for passive tracers in turbulent fluids and consistent with previous results in literature. In Section 2, we describe the data set along with a brief introduction to the analysis methodology used, the so-called diffusion entropy analysis (DEA; Scafetta & Grigolini 2002). Section 3 is devoted to the description of our results, which are discussed in Section 4. In Section 5 we provide conclusions and outline future prospects.

2. Observations and Data Analysis

2.1. The Data Set

The data set used in this work consists of seven different time series of magnetograms with different fields of view (FoVs) acquired by the *Hinode* mission (Kosugi et al. 2007; Tsuneta et al. 2008) in 2010 and targeted at the disk center. All the time series were acquired in the framework of the *Hinode* Operation Plan 151 (HOP151) entitled "Flux replacement in the network and internetwork," and are listed in Table 1. The magnetogram time series share a common spatial resolution of $\sim 0\farcs3$, and a noise level of ~ 4 G on average. For each FoV the noise was estimated from the rms values in a region free of magnetic signal, and convolved with a 3×3 pixel^2 spatial kernel corresponding to a truncated Gaussian with an FWHM of 2 pixels, as explained in detail in Gošić et al. (2014). The duration and time cadence of each magnetogram time series are listed in Table 1. All the data were filtered out to account for acoustic oscillations at 3.3 mHz. In Figure 1 we show the mean magnetograms averaged over the whole observation time for each of the time series listed in Table 1.

Table 1
Magnetogram Time Series Used

FoV ID	Duration (hr)	Time Cadence (s)	Tracked MEs	Maximum Lifetime (hr)
JAN 1	11.1	60	17,189	8.9
JAN 2	8.4	60	12,555	7.1
FEB	25.6	120	15,376	17.1
APR	28.9	80	24,958	8.9
DEC 1	17.2	90	14,524	11.1
DEC 2	18.6	90	15,714	12.5
NOV	24.0	90	20,145	9.3

The segmentation of each magnetogram in the series listed above was performed as explained in Giannattasio et al. (2013). The iterative procedure described there used an adaptive threshold in order to limit the loss of weak features and the merging of different features in big clusters (Berrilli et al. 2005). The MEs were identified and tracked using the algorithm described in Del Moro (2004). According to this, only the trajectories of MEs living for more than four subsequent frames were used to perform the analysis described below. In the fourth column of Table 1 we report the number of tracked MEs actually analyzed into each one of the listed FoVs. A total of 120,461 MEs were tracked in the quiet Sun at the disk center, with their lifetimes ranging from $\simeq$5 minutes to $\simeq$17.1 hr. Of course, the shortest lifetimes are biased by the selection criteria used.

We remark that such a huge number of MEs is being tracked for the first time to perform studies inherent to the dynamic properties of the quiet photosphere. Moreover, the analysis of different FoVs acquired in different time windows allows us to determine if the turbulent regime emerging from the motion of MEs is a common property of the quiet Sun or if it depends on the peculiar physical conditions found over time.

2.2. Diffusion Entropy Analysis (DEA)

The displacements of all the N MEs in the HOP151 data set, namely $|\boldsymbol{x}_n(t)|$ $(n = 1, 2, \ldots, N)$, can be considered as the time series of which we want to investigate the scaling properties. Given a set of N trajectories we consider the probability distribution function (PDF) of observing the displacement x at time t, namely $p(x, t)$. For a stationary and scale-invariant process, the following relation holds:

$$p(x, t) = t^{-\delta} G(xt^{-\delta}), \tag{3}$$

where δ is a scaling exponent, and G is a smooth function. In this case, some constraints on the dynamic properties of the system can be recovered by measuring δ with the best precision. For example, it is well known that in the case of a pure random walk (RW) the function G is expected to be a Gaussian, and $\delta = 0.5$. Scafetta & Grigolini (2002) proposed an analysis technique based on the Shannon entropy to evaluate δ with high precision, namely the DEA. The Shannon entropy S

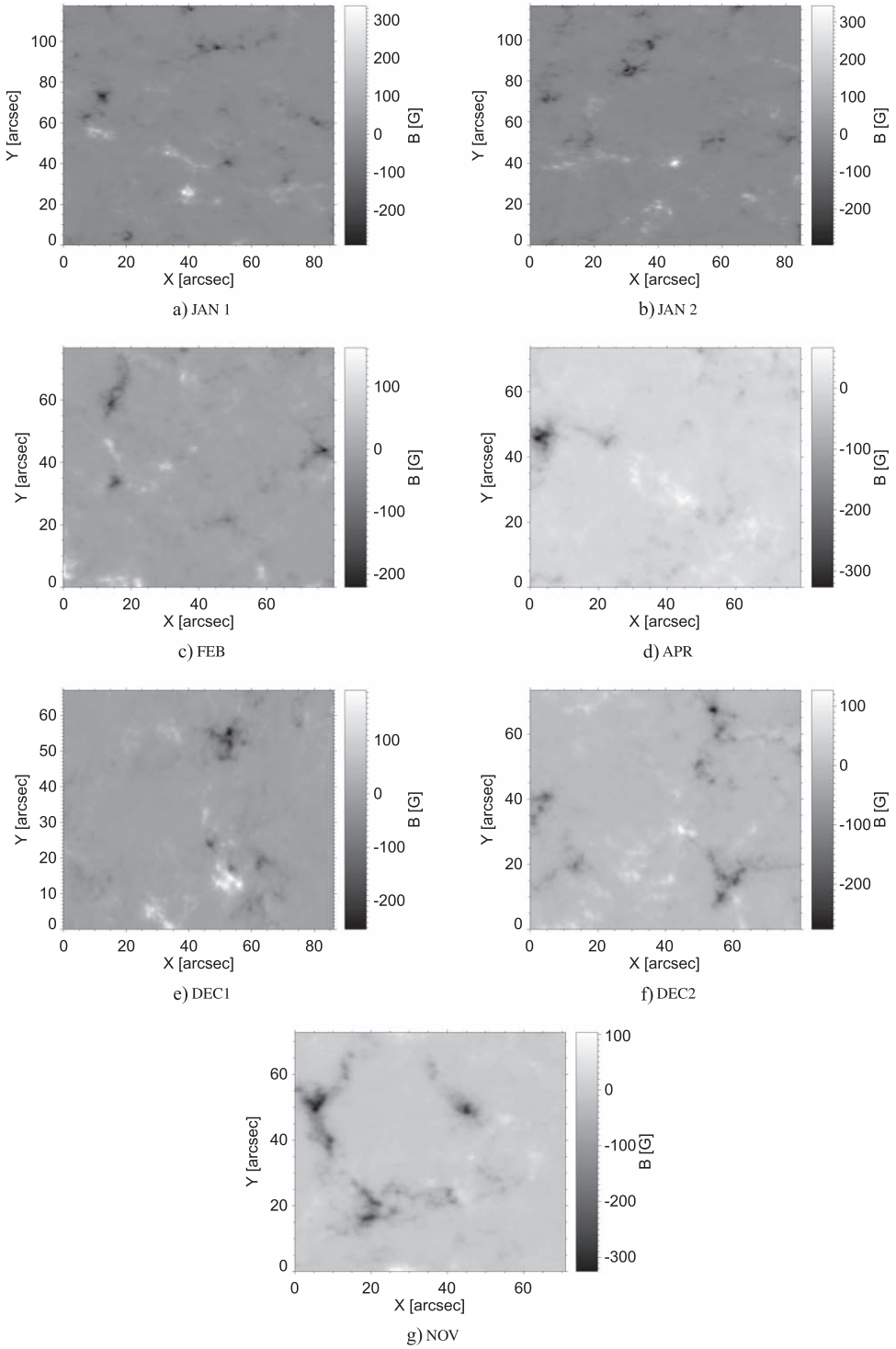

Figure 1. Average magnetogram of the seven FoVs representing the data set used in this work and listed in Table 1. Aspect ratios have been modified to fit all the panels to the page.

(t) of a process described by the PDF $p(x, t)$ is defined as

$$S(t) = -\int_{-\infty}^{\infty} p(x, t)\ln[p(x, t)]dx. \quad (4)$$

When $p(x, t)$ satisfies the condition in Equation (3) and Equation (4) becomes

$$S(t) = \delta \ln(t) + A, \quad (5)$$

with

$$A = -\int_{-\infty}^{\infty} G(w)\ln[G(w)]dw, \qquad w = xt^{-\delta}.$$

We note from Equation (5) that $S(t)$ increases linearly with $\ln(t)$, the slope δ being the scaling exponent. This means that when $p(x, t)$ is available, it is possible to compute $S(t)$ using Equation (4), and subsequently δ as the slope in a semi-log plot $\ln(t)$ versus $S(t)$. The error on $S(t)$ and δ may be computed as

follows. The PDF in the ith displacement bin of size Δx, namely $p_i(x, t)$, is evaluated as the number of MEs, N_i, who displaced a quantity between $x - \Delta x/2$ and $x + \Delta x/2$ at time t, normalized by $N_{\rm TOT}$, the total number of MEs statistically contributing to $_{pi}$, i.e., the number of MEs aged at least that time

$$p_i(x, t) = \frac{N_i}{N_{\rm TOT}}.$$

Under the hypothesis that the uncertainty on $p_i(x, t)$ is governed by Poisson statistics, we have

$$\Delta p_i(x, t) = \frac{\sqrt{N_i}}{N_{\rm TOT}}.$$

Following the definition of $S(t)$ in Equation (4), the error on the entropy, $\Delta S(t)$, was computed as

$$\Delta S(t) = \int_{-\infty}^{\infty} \Delta p_i |\ln(p_i)| dx + \int_{-\infty}^{\infty} \Delta p_i dx. \quad (6)$$

The error on the slope was computed as the error on the fit obtained by weighting any data point by the inverse error on entropy.

3. Results

We applied the DEA technique described in Section 2.2 to the ME trajectories tracked in the data sets listed in Table 1, and computed the entropy $S(t)$ for any time series, by following the definition in Equation (4). The results are shown in panels (a)–(g) of Figure 2 (black diamonds). In the same figure, the black vertical lines represent the error on the entropy, which was computed using Equation (6). The dashed red lines with slope δ correspond to the best fit of $S(t)$ versus $\log(t)$ as indicated by Equation (5) up to $t \sim 2000$ s, the time at which the fit in the DEC2 FoV starts to no longer be excellent. This is probably due to the joint action of the decreasing statistics of MEs living for longer and longer times together with the fact that DEC2 FoV has the higher percentage of tracked MEs (over 5.15%) with average magnetic field strength above the equipartition value, i.e., 255 G (Giannattasio et al. 2013). These MEs experience a dynamic regime slowed down by their resistance to the underlying flow, and are perhaps part of network regions, although in the FoVs analyzed here it is not possible to distinguish among network and internetwork regions, with the only exception being NOV.

We checked for the existence of different slopes in the trends shown instead of a single one by computing the second derivative of entropy, namely $S'' = d^2S(t)/d(\ln(t))^2$, for $t \lesssim 2000$ s. As S'' tightly oscillates about zero, we conclude that no significant different regimes emerge with DEA over the timescales considered in this analysis.

We recall that the slope δ can be interpreted as the scaling exponent of PDFs describing the statistical properties of stationary and scale-invariant displacement of MEs in the quiet Sun. This exponent, in our case, ranges between $\simeq$0.58 (for the data set tagged as FEB) and $\simeq$0.63 (for the data set tagged as DEC1), with a mean value of $\langle\delta\rangle = 0.60 \pm (0.02^{(p)}, 0.01^{(s)})$, where the superscripts (p) and (s) indicate the propagated and the standard error, respectively. It is important to note that different data sets, acquired at the disk center in different months, with different cadence, and characterized by different magnetic flux coverage and spatial distribution, agree in providing consistent values of δ within the error. Thus, it is reasonable to consider all the MEs tracked to perform the DEA analysis on a number of ME trajectories much higher than that in the case of single FoVs listed in Table 1.

The bottom right panel of Figure 2 shows $S(t)$ versus $\ln(t)$ for the data set tagged as ALL, i.e., when considering all the MEs tracked in this work. The slope of the linear trend, computed as explained above for the single data sets, is $\delta_{\rm ALL} = 0.62 \pm 0.04$. This value, within the error, is consistent with the values of the single slopes obtained for each FoV, and with their average $\langle\delta\rangle$, it thus can be considered reliably representative of the quiet Sun.

4. Discussion

4.1. Stationarity of ME Displacement Time Series

It is well known that nonlinear analysis effectively describes the behavior of complex systems that are out of equilibrium and show correlations on a wide range of spatiotemporal scales. One fundamental hypothesis when investigating complex systems like the turbulent solar photosphere in the quiet Sun via the scaling analysis is that the time series under investigation, $x(t)$ are stationary in some sense. This hypothesis is also the basis of the DEA technique.

In order to check the stationarity of our time series we performed the Augmented Dickey–Fuller test (ADF; see, e.g., Fuller 1977; Said & Dickey 1984; Elliott et al. 1996). Let us suppose that the stochastic process describing the displacement of MEs can be modeled as an autoregressive process Y_t of order p with a trend $\alpha + \beta t$, namely

$$Y_t = \alpha + \beta t + a_1 Y_{t-1} + a_2 Y_{t-2} + ... + a_p Y_{t-p} + \varepsilon_t, \quad (7)$$

where α is a constant, β is the parameter of the linear trend, p is the lag order of the autoregressive model, $(a_1, \ldots, a_p)$ is a set of weights, and ε_t is the stochastic variable mimicking a stochastic process with zero mean and constant variance. We note that the case $\alpha = \beta = 0$ corresponds to an RW. By using a backshift operator $B(Y_t) = Y_{t-1}$ we can associate the *characteristic polynomial*

$$1 - a_1 B - a_2 B^2 - ... - a_p B^p - \alpha - \beta t \quad (8)$$

and the *characteristic equation*

$$1 - a_1 B - a_2 B^2 - ... - a_p B^p - \alpha - \beta t = 0. \quad (9)$$

The model can be expressed in terms of first differences $\Delta Y_t = Y_t - Y_{t-1}$ and a single-lagged level Y_{t-1} as

$$\Delta Y_t = \gamma Y_{t-1} + a_1 \Delta Y_{t-1} + a_2 Y_{t-2} + ... + a_p Y_{t-p} + \alpha + \beta t + \varepsilon_t. \quad (10)$$

For example, for $p = 2$

$$Y_t = a_1 Y_{t-1} + a_2 Y_{t-2} + \alpha + \beta t + \varepsilon_t, \quad (11)$$

from which

$$\Delta Y_t = (a_1 + a_2 - 1) Y_{t-1} - a_2 \Delta Y_{t-1} + \alpha + \beta t + \varepsilon_t, \quad (12)$$

where $\gamma = a_1 + a_2 - 1$ is the coefficient of the single-lagged term. Note that γ is the negative of the characteristic polynomial evaluated at the unit root $B = 1$. It can be shown that if the characteristic equation has a unit root, then the time series is nonstationary. This satisfies the null hypothesis that the coefficient of the single-lagged level Y_{t-1} is zero. In other

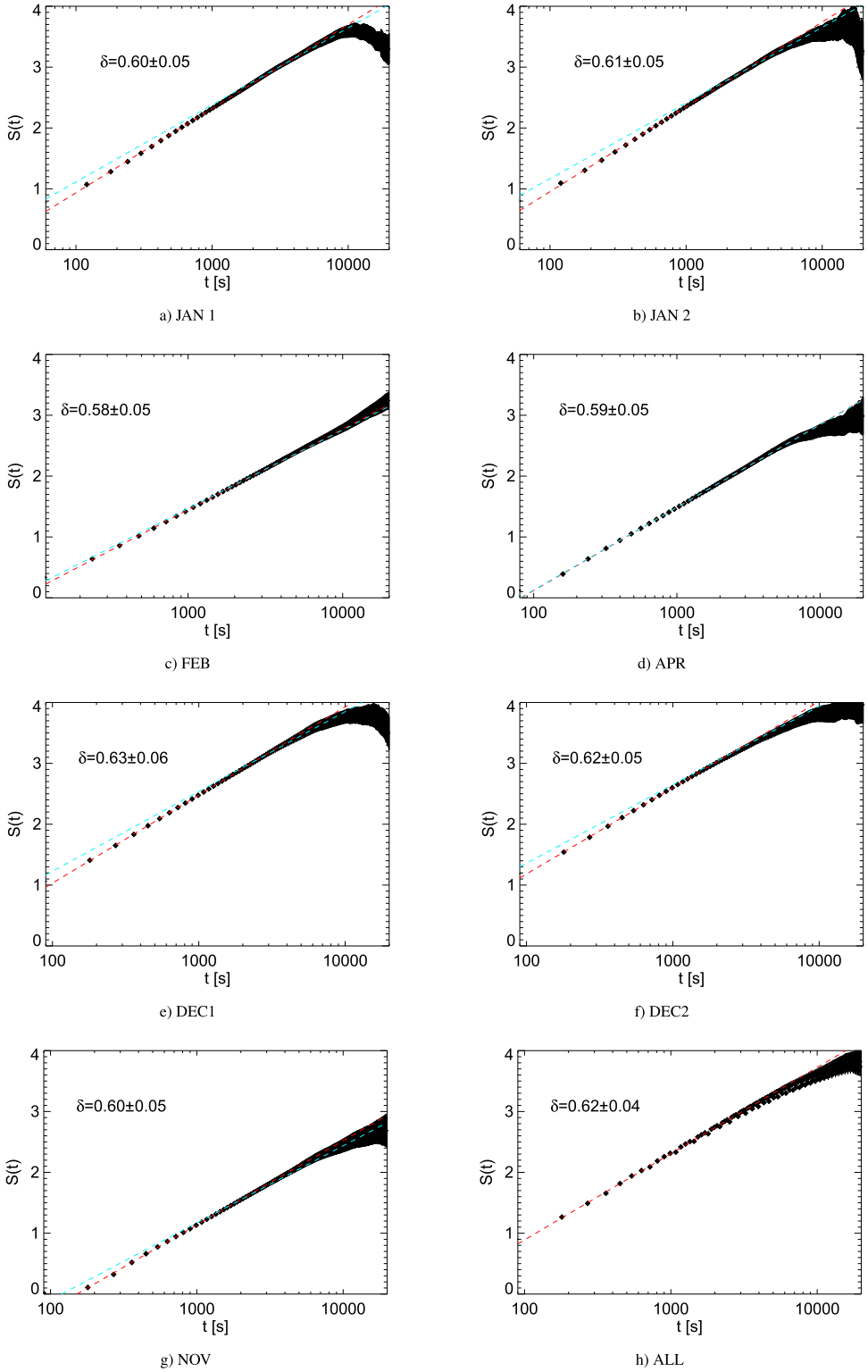

Figure 2. $S(t)$ (black diamonds) as computed following Equation (4). The vertical bars (where visible) represent the errors $\Delta S(t)$ computed as explained in Section 2.2. The dashed red line with slope δ corresponds to the best fit up to $t \sim 2000$ s in a $S(t)$ vs. $\log(t)$ plot. The dashed cyan line corresponds to the values of $\delta_{t>2000s}$ obtained from Equation (23) after computing $\gamma = 2H$, as explained in Section 4.4).

words, nonstationarity corresponds to having one or more unit roots in the characteristic polynomial. The ADF basically tests this null hypothesis. The logic here is that if a time series Y_t is stationary in some sense, then it tends to return to a certain mean value or trend, such that large (small) values are likely to be followed by small (large) values and so on. For this reason, it is necessary that the model at time t has a statistically negative coefficient for the term Y_{t-1}, namely $\gamma < 0$. The more negative this coefficient is, below a threshold θ that depends on

the number of samples and the confidence level required, the more likely that it has a stationary time series.

We performed the ADF test for the ME displacement time series used in this work using the Python routine *adfuller*, which takes advantage of the autoregressive model with the trend described by Equation (7) and the automatic search for the number of lags according to the Akaike Information Criterion (Akaike 1974; Burnham & Anderson 2002). We found that the null hypothesis can be discarded with a confidence level >99% (according to the tabled values computed by MacKinnon 1994). In fact, we found for the longest time series a coefficient $\gamma < -5$, with the threshold $\theta \simeq -3.44$. Thus, with $\gamma < \theta$ we can reject the null hypothesis and consider the displacement time series of the MEs tracked, $x(t)$, as stationary with a very high confidence level.

4.2. DEA and the Scaling Exponent of ME Displacement

The study of the statistical properties of ME displacements under the hypothesis that MEs are passively transported by the photospheric plasma flow is the only reliable way to capture and constrain some aspects inherent to the plasma velocity field in the quiet Sun, which are directly related to the appearance of the observed features at all spatiotemporal scales, from subgranular to global. The turbulent photosphere is a complex (and actually very complicated) system, and nonlinear dynamics comes as its natural framework within which to describe the appearance and mixing of different spatiotemporal scales. Furthermore, in this kind of system the only quantities often considered to be relevant are those characterizing the dynamics in a statistical sense, rather than detailing the behavior of single particles. In this view, studying the statistics of MEs displacement allows us to approach turbulent convection by taking advantage of real observations instead of simulations or (still lacking) theoretical models. This motivates the analysis proposed in this work.

Since the pioneering works of Berger et al. (1998), Cadavid et al. (1998, 1999), Hagenaar et al. (1999), Lawrence et al. (2001), and Abramenko et al. (2011), nonlinear techniques have been successfully used to investigate the dynamic properties of MEs in the quiet Sun. These studies basically made use of the first two momenta of the PDFs of displacements. The diffusion entropy analysis proposed in this work takes advantage of dealing with the PDFs of the displacement x instead of its momenta, directly providing their scaling properties and identifying their dynamic regimes without the intermediate step of retrieving them from higher momenta. In fact, it is customary to express the scaling properties by means of the relation $x \propto t^{\delta}$, retrieve the second momentum $\langle x^2 \rangle$, and suppose it is proportional to $t^{2\delta}$. However, the identification of the second-order momentum exponent with two times the scaling exponent is not strictly correct in general, and is verified only in the Gaussian case, for which the displacement

$$x(t) = x(0) + \int_0^t dt' \xi(t') \tag{13}$$

is characterized by the Gaussian fluctuation $\dot{x(t)} = \xi(t)$. In all the other cases, the scaling of the second-order moment should be indicated as $\langle x^2 \rangle \propto t^{2H}$, where H is the Hurst exponent (Hurst 1956). In other words, while in general $H \neq \delta$, in the Gaussian case it can be demonstrated that $\delta = H = 0.5$.

As we are in the presence of dynamic regimes characterized by a scaling index of the PDFs of displacements with $\delta > 0.5$, we confirm that MEs in the quiet Sun unequivocally undergo a superdiffusive regime. This implies, in accordance with previous results in the literature, that the diffusion rate is not constant at all on the spatial and temporal scales, but is smaller at the smaller scales and greater at the greater scales (see, e.g., Abramenko et al. 2011). As a consequence, the amplification of the magnetic field in the photosphere is more likely to occur at smaller scales, where it can more effectively resist the sweeping action of the underlying turbulent plasma flow.

The results shown in this work are very important, as they also suggest that MEs in the quiet Sun show the same dynamic properties, regardless of the specific environment in which they are embedded, which correspond to the dynamic properties of turbulent convection when it is assumed that they are passively transported by the plasma velocity field. By taking advantage of a very robust statistics (the total number of tracked MEs is 120,461) we found $\langle \delta \rangle = 0.60 \pm 0.02$ when considering the average δ computed over the single FoVs and retaining the propagated error as the worst case, and $\delta_{\rm ALL} = 0.62 \pm 0.04$ when considering the δ computed from the extended set of trajectories of all the MEs from all the FoVs. Regarding the latter, one could object that this value was obtained by mixing trajectories retrieved from time series of magnetograms with different cadences, thus there is not a significant improvement in the statistics, as some discrete times could be undersampled with respect to other ones. However, the number of samples at each time step impacts the definition of $\Delta p_i(x, t)$, and is taken into account in evaluating the error on $S(t)$ according to Equation (6), which ultimately contributes to evaluation of the error on the slope $\delta_{\rm ALL}$. Moreover, there is not a clear correlation among the time cadence of the time series and the retrieved δ for any subset listed in Table 1. In light of these considerations, both values $\langle \delta \rangle$ and $\delta_{\rm ALL}$ are fully consistent, and thus represent the scaling properties of the PDFs of ME displacement in the quiet Sun.

4.3. Lévy Walks and the Motion of MEs

One of the most studied dynamic regimes fulfilling the relations $\delta \neq H$, $\delta > 0.5$ is represented by the Lévy diffusion processes (Lévy 1937), which correspond to RWs in which the distribution of fluctuations (let us term them *jumps* in this special case) is heavy-tailed. In particular, in Lévy processes the tail of the jump (ξ) distribution follows a power law. Among these processes, observed in many different complex systems in nature (from the flight of birds to the shark haunting strategy to the behavior of the financial markets, or the heartbeat rhythm in the presence of hearth disease, just to mention a few), we will distinguish between *Lévy flights* and *Lévy walks* (see, e.g., Shlesinger et al. 1987, 1993). The former are the result of aleatory jumps with size being independent and identically distributed with infinite variance, thus violating the Central Limit Theorem (CLT). In these flights the walker visits only the start and the end points of the paths, and not the intermediate points. On the other hand, Lévy walks are characterized by constant velocities, and all the intermediate points of a jump are visited by the walker. In a Lévy flight the distribution of jumps is given by

$$P(\xi \leqslant x) = \int_0^x p(x')dx' \propto x^{-\alpha}, \tag{14}$$

for which the PDF of displacements x is given by

$$p(x) \propto x^{-(\alpha+1)}, \tag{15}$$

where the condition $0 < \alpha < 2$ holds to give an infinite variance for the distribution of jumps ξ. In the case of stable and symmetric ξ distributions, for which the frequency of long jumps is the same for both positive and negative increments (which cause approach and departure from the initial position, respectively) the characteristic function of $p(x)$, namely its Fourier transform, is given by (Shlesinger et al. 1993)

$$\hat{p(k)} = e^{-b|k|^{\alpha}}, \tag{16}$$

where $|k| \propto 1/|x|$, and the parameter b is a measure of the strength of the diffusion process. With the position $\mu = \alpha + 1$ it follows that Equation (16) can be written as

$$\hat{p(k)} = e^{-b|k|^{\mu-1}}, \tag{17}$$

with $\mu < 3$. For stable distributions the generalized CLT provides, for the characteristic function of $p(x, t)$

$$\hat{p(k}, t) = e^{-b|k|^{\mu-1}t}. \tag{18}$$

In this case, the inverse Fourier transform gives a $p(x, t) \propto x^{\delta}$, with

$$\delta = \frac{1}{\mu - 1}, \tag{19}$$

which is well defined even if the second-order moment diverges and H cannot be defined satisfactorily. Thus, a Lévy flight satisfies the inequality $\delta \neq H$, but is difficult to interpret from a physical point of view.

In this context, the Lévy walk was introduced to deal with more meaningful situations in which particles cannot actually perform instantaneous very long jumps, but such extreme jumps take a time proportional to their length (Shlesinger et al. 1987, 1993). The basic assumptions made are that: (i) the travel time τ between following jumps is governed by the PDF $\Psi(\tau)$; and (ii) the PDF of the variable collecting the fluctuation has no more a stable form, but is asymptotically expressed by an inverse power law $p(x) \propto |x|^{-\mu}$. These two prescriptions, together with the normalization condition, provide an analytical expression for $\Psi(\tau)$ (Grigolini et al. 2001; Scafetta & Grigolini 2002), namely

$$\Psi(\tau) = (\mu - 1)\frac{T^{\mu-1}}{(T + \tau)^{\mu}}, \tag{20}$$

where T is a constant. The condition $\mu > 2$ ensures that it is possible to define a finite mean travel time

$$\langle \tau \rangle = \int_{-\infty}^{\infty} \tau' \Psi(\tau') d\tau' = \frac{T}{\mu - 2}. \tag{21}$$

Also, in this instance the quantity μ should remain <3. In fact, the values $\mu \geqslant 3$ bring us again to the Gaussian case. Thus, for a Lévy walk, the condition $2 < \mu < 3$ must be fulfilled. But, importantly, this time the second-order moment of the displacement PDF is finite, and it can be demonstrated that (Scafetta & Grigolini 2002)

$$H = \frac{4 - \mu}{2}, \tag{22}$$

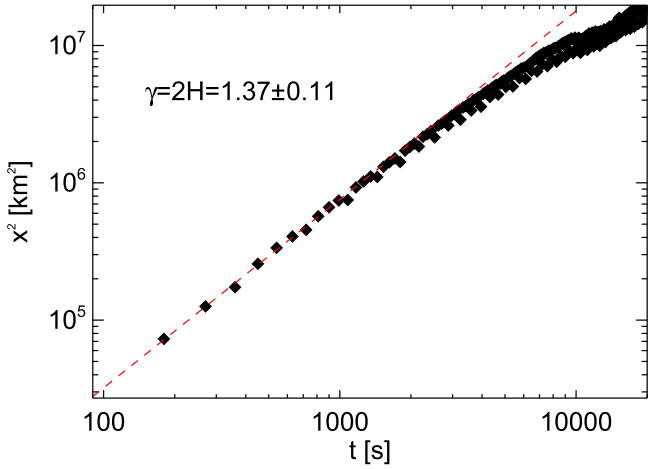

Figure 3. Mean-square displacement of all the MEs in the data set. To be consistent with the works of Giannattasio and collaborators (see the text), the spectral index in those works corresponds to two times the Hurst exponent, namely $\gamma = 2H$.

which together with Equation (19) (which is still valid) leads to

$$\delta = \frac{1}{3 - 2H}. \tag{23}$$

This equation is important for two reasons. First, it demonstrates that in general there exist dynamic regimes for which $\delta \neq H$; and second, it relates the spectral index H of the displacement spectra with the scaling exponents of the displacement PDFs in the case of dynamic regimes ascribable to Lévy walks.

The hypothesis that the motion of MEs in the quiet Sun follows a Lévy walk dynamics can be checked by taking advantage of Equation (23). In previous works, Giannattasio and collaborators studied the displacement spectrum of MEs, namely the behavior of $\langle x^2(t) \rangle \propto t^{\gamma}$, in the data set tagged as NOV in Table 1 (Giannattasio et al. 2013, 2014b). They found a spectral index $\gamma = 1.34 \pm 0.02$ for times $\lesssim$2000 s. As γ was computed from the time scaling of the mean-square displacement (i.e., the second-order moment of the displacement distribution), it can be identified with twice the Hurst exponent, as explained above, and the relation $\gamma = 2H$ holds. Within the error, the substitution of $2H = 1.34 \pm 0.02$ in Equation (23) produces a scaling index δ ranging between 0.59 and 0.61. On the other hand, the scaling exponent inferred with the DEA technique for the same data set is $\delta = 0.60 \pm 0.05$ (panel (g) of Figure 2), which is consistent with the value provided by Equation (23). As a further check, we computed the displacement spectrum for the whole data set in Table 1 (tagged as ALL throughout the text), applying the same algorithm used in Giannattasio et al. (2013, 2014b) and references therein. We obtained a spectral index $2H = 1.37 \pm 0.11$ (Figure 3). Within the error, the substitution of this value in Equation (23) produces a scaling index in the range $0.57 \leqslant \delta \leqslant 0.66$. The scaling exponent found by performing the DEA analysis is $\delta = 0.62 \pm 0.04$ (bottom right panel of Figure 2), which, again, is consistent with the value provided by Equation (23). This is an important result and suggests that the diffusion of MEs in the quiet Sun is driven by dynamical processes that are fully consistent with a Lévy walk description. This enhanced diffusion regime is well known to arise in other complex systems and to be associated with chaos-

induced turbulent diffusion, the diffusion of Brownian particles in shear flows, the diffusion of passive scalars in a turbulent flow, and in turbulent regimes characterized by intermittency.

4.4. Final Remarks

In previous works, Giannattasio and collaborators analyzed the diffusion properties of the ME trajectories in the data set tagged as NOV in Table 1 (Giannattasio et al. 2013, 2014b). They found that MEs undergo an anomalous diffusion with a change in the slope $\gamma = 2H$ at $t \sim 2000$ s, when the transport regime changes from a stronger to a weaker (quasi-normal) superdiffusion, suggesting a difference in the dynamic properties of MEs living inside and on the boundaries of the supergranular cell entirely enclosed in the FoV. The authors argued that this is mainly due to different magnetoconvection regimes occurring in the photospheric plasma by moving from the internetwork to the network regions, as the magnetic flux becomes stronger, more correlated, and longer-lived. To be conservative and consistent with the hypothesis of MEs passively transported by the flow, which is strictly valid only for internetwork MEs, when applying DEA, the fit of $S(t)$ versus $\log(t)$ is computed up to $\tau \sim 2000$ s. As we can see, $S(t)$ is well fitted by a single slope, at least up to the timescales where the statistics is still robust and the error on $S(t)$ is still not appreciable, say, up to $\sim$6000 s. This may be explained by taking into account two factors.

(1) As argued in Section 4.2 there is a conceptual difference among the scaling exponent of the displacement spectra, γ, and the scaling of the PDFs of displacement, δ, thus all the features emerging from the former may have not a bijective correspondence with those emerging from the latter, as in general $\delta \neq H$. For Lévy walk dynamics the consistency among the two results should be checked via Equation (23).

(2) At longer scales, and with the worsening of the statistics, the DEA might be less sensitive to slight changes of the slope γ. Giannattasio et al. (2013) observed a γ transition at $t \sim 2000$ s from $\gamma \simeq 1.34$ to $\gamma \simeq 1.20$. When applying Equation (23), we find that the former is perfectly consistent with the δ computed with DEA and shown in panel (g) of Figure 2; the latter corresponds to a value of $\delta = 0.55$ for $t > 2000$ s, which is shown as a cyan dashed line in the same figure. The same applies to all the other data sets as well. In fact, for each of them we computed the slopes γ and found that for $t \lesssim 2000$ s they are consistent with the δ computed with DEA, and for $t \gtrsim 2000$ they correspond to the δ values represented as cyan dashed lines in Figure 2. Within the errors on $S(t)$ and δ, these close values provide very close fitting lines for $t > 2000$ s. In particular, the cyan lines appear to be buried in the error of $S(t)$, such that both γ slopes are simultaneously consistent with DEA results. In this sense DEA may be less sensitive to changing slopes, so we preferred to be conservative and fit the trend at all times with a single-slope line. But this is not in contrast with the double-slope behavior detected in previous works, which is supported by these two considerations.

5. Conclusions

Many aspects inherent to turbulent convection in action in the outermost layer of the solar radius are still obscure. It is not clear, for example, what are the mechanisms triggering such turbulent behavior, even if there are robust indications that it cannot be ascribed to Kolmogorov–Kraichnan scalings or MHD turbulence models.

In this paper, we have demonstrated that the motion of MEs in the quiet Sun, which can be used as tracers of the underlying plasma flow, is consistent with a Lévy walk dynamic regime with the same dynamic properties regardless of the specific environment. This is important for shedding light on the mechanisms and the scales at which turbulent convection operates in the solar photosphere, and for providing some constraints for the models attempting to explain the heating of the upper atmosphere. Our next work will be devoted to the investigation of the intermittent character of ME motion in the quiet Sun as an important characteristic of turbulence.

We believe that studies of turbulent convection, as well as studies of the characteristic scales of evolution and organization of magnetic fields in the quiet Sun, could greatly benefit from the information gained from the diffusion entropy analysis proposed here. Due to its high reliability and simple implementation, we suggest this entropy-based method be extensively employed in the study of the spatial and temporal scales involved in the evolution of both photospheric plasma and MEs.

F.G. is grateful to M. Gošić and L. Bellot Rubio for providing the data analyzed here. This paper is based on data acquired in the framework of the *Hinode* Operation Plan 151 entitled "Flux replacement in the network and internetwork." *Hinode* is a Japanese mission developed and launched by ISAS/JAXA, collaborating with NAOJ as a domestic partner, and NASA and STFC (UK) as international partners. Scientific operation of the *Hinode* mission is conducted by the *Hinode* science team organized at ISAS/JAXA. This team mainly consists of scientists from institutes in the partner countries. Support for the post-launch operation is provided by JAXA and NAOJ (Japan), STFC (U.K.), NASA, ESA, and NSC (Norway).

ORCID iDs

F. Giannattasio https://orcid.org/0000-0002-9691-8910
G. Consolini https://orcid.org/0000-0002-3403-647X
F. Berrilli https://orcid.org/0000-0002-2276-3733

References

Abramenko, V. I. 2017, MNRAS, 471, 3871
Abramenko, V. I. 2018, MNRAS, 480, 1607
Abramenko, V. I., Carbone, V., Yurchyshyn, V., et al. 2011, ApJ, 743, 133
Agrawal, P., Rast, M. P., & Gošić, M. 2018, ApJ, 854, 118
Akaike, H. 1974, ITAC, 19, 716
Alfvén, H. 1947, MNRAS, 107, 211
Beeck, B., Collet, R., Steffen, M., et al. 2012, A&A, 539, A121
Berger, T. E., Löfdahl, M. G., Shine, R. A., & Title, A. M. 1998, ApJ, 506, 439
Berrilli, F., Consolini, G., Pietropaolo, E., et al. 2002, A&A, 381, 253
Berrilli, F., Del Moro, D., Consolini, G., et al. 2004, SoPh, 221, 33
Berrilli, F., del Moro, D., Florio, A., & Santillo, L. 2005, SoPh, 228, 81
Berrilli, F., Florio, A., Consolini, G., et al. 1999, A&A, 344, L29
Berrilli, F., Scardigli, S., & Del Moro, D. 2014, A&A, 568, A102
Berrilli, F., Scardigli, S., & Giordano, S. 2013, SoPh, 282, 379
Brandt, P. N., & Getling, A. V. 2008, SoPh, 249, 307
Burnham, K., & Anderson, D. 2002, Model Selection and Multimodel Inference: A Practical Information-theoretic Approach (Verlag: Springer)
Cadavid, A. C., Lawrence, J. K., & Ruzmaikin, A. A. 1999, ApJ, 521, 844
Cadavid, A. C., Lawrence, J. K., Ruzmaikin, A. A., Walton, S. R., & Tarbell, T. 1998, ApJ, 509, 918
Caroli, A., Giannattasio, F., Fanfoni, M., et al. 2015, JPlPh, 81, 495810514
Cattaneo, F., Emonet, T., & Weiss, N. 2003, ApJ, 588, 1183

Centeno, R., Socas-Navarro, H., Lites, B., et al. 2007, ApJL, 666, L137
Consolini, G., Carbone, V., Berrilli, F., et al. 1999, A&A, 344, L33
Danilovic, S., Cameron, R. H., & Solanki, S. K. 2015, A&A, 574, A28
De Pontieu, B., McIntosh, S. W., Carlsson, M., et al. 2007, Sci, 318, 1574
de Wijn, A. G., Lites, B. W., Berger, T. E., et al. 2008, ApJ, 684, 1469
Del Moro, D. 2004, A&A, 428, 1007
Del Moro, D., Berrilli, F., Duvall, T. L., Jr., & Kosovichev, A. G. 2004, SoPh, 221, 23
Del Moro, D., Giannattasio, F., Berrilli, F., et al. 2015, A&A, 576, A47
Elliott, G., Rothenberg, T. J., & Stock, J. H. 1996, Econometrica, 64, 813
Fuller, W. A. 1977, Journal of the Royal Statistical Society. Series A (General), 140, 379
Getling, A. V. 2006, SoPh, 239, 93
Getling, A. V., & Brandt, P. N. 2002, A&A, 382, L5
Giannattasio, F., Berrilli, F., Biferale, L., et al. 2014a, A&A, 569, A121
Giannattasio, F., Berrilli, F., Consolini, G., et al. 2018, A&A, 611, A56
Giannattasio, F., Del Moro, D., Berrilli, F., et al. 2013, ApJL, 770, L36
Giannattasio, F., Stangalini, M., Berrilli, F., Del Moro, D., & Bellot Rubio, L. 2014b, ApJ, 788, 137
Gošić, M., Bellot Rubio, L. R., del Toro Iniesta, J. C., Orozco Suárez, D., & Katsukawa, Y. 2016, ApJ, 820, 35
Gošić, M., Bellot Rubio, L. R., Orozco Suárez, D., Katsukawa, Y., & del Toro Iniesta, J. C. 2014, ApJ, 797, 49
Grigolini, P., Palatella, L., & Raffaelli, G. 2001, Fract, 09, 439
Hagenaar, H. J., Schrijver, C. J., Title, A. M., & Shine, R. A. 1999, ApJ, 511, 932
Hanasoge, S. M., Duvall, T. L., & Sreenivasan, K. R. 2012, PNAS, 109, 11928
Hart, A. B. 1956, MNRAS, 116, 38
He, X., Funfschilling, D., Nobach, H., Bodenschatz, E., & Ahlers, G. 2012, PhRvL, 108, 024502
Hurst, H. E. 1956, Proceedings of the Institution of Civil Engineers, 5, 1753
Jefferies, S. M., McIntosh, S. W., Armstrong, J. D., et al. 2006, ApJL, 648, L151
Keys, P. H., Mathioudakis, M., Jess, D. B., Mackay, D. H., & Keenan, F. P. 2014, A&A, 566, A99
Kosugi, T., Matsuzaki, K., Sakao, T., et al. 2007, SoPh, 243, 3
Lawrence, J. K., Cadavid, A. C., Ruzmaikin, A., & Berger, T. E. 2001, PhRvL, 86, 5894
Lepreti, F., Carbone, V., Abramenko, V. I., et al. 2012, ApJL, 759, L17
Lévy, P. 1937, Théorie de l'addition des Variables Aléatoires (Paris: Gauthier-Villars)
MacKinnon, J. G. 1994, Journal of Business and Economic Statistics, 12, 167
Manso Sainz, R., Martínez González, M. J., & Asensio Ramos, A. 2011, A&A, 531, L9
Nesis, A., Hammer, R., Roth, M., & Schleicher, H. 2006, A&A, 451, 1081
Niemela, J. J., Skrbek, L., Sreenivasan, K. R., & Donnelly, R. J. 2000, Natur, 404, 6780
Nordlund, A., & Stein, R. 1997, in SCORe'96: Solar Convection and Oscillations and their Relationship, ed. F. P. Pijpers, J. Christensen-Dalsgaard, & C. S. Rosenthal (Dordrecht: Springer), 79
November, L. J. 1980, PhD thesis, Colxorado Univ., Boulder
Orozco Suárez, D., Katsukawa, Y., & Bellot Rubio, L. R. 2012, ApJL, 758, L38
Parker, E. N. 1957, JGR, 62, 509
Parker, E. N. 1988, ApJ, 330, 474
Petrovay, K. 1994, in NATO Advanced Science Institutes (ASI) Series C, ed. R. J. Rutten & C. J. Schrijver (Dordrecht: Springer), 415
Petrovay, K., & Szakaly, G. 1993, A&A, 274, 543
Rast, M. P. 2002, A&A, 392, L13
Rempel, M., Schüssler, M., Cameron, R. H., & Knölker, M. 2009, Sci, 325, 171
Roudier, T., Malherbe, J. M., Rieutord, M., & Frank, Z. 2016, A&A, 590, A121
Roudier, T., Malherbe, J. M., Vigneau, J., & Pfeiffer, B. 1998, A&A, 330, 1136
Said, S. E., & Dickey, D. A. 1984, Biometrika, 71, 599
Sánchez Almeida, J., Bonet, J. A., Viticchié, B., & Del Moro, D. 2010, ApJL, 715, L26
Scafetta, N., & Grigolini, P. 2002, PhRvE, 66, 036130
Shlesinger, M. F., West, B. J., & Klafter, J. 1987, PhRvL, 58, 1100
Shlesinger, M. F., Zaslavsky, G. M., & Klafter, J. 1993, Natur, 363, 31
Simon, G. W., & Leighton, R. B. 1964, ApJ, 140, 1120
Sobotka, M., Švanda, M., Jurčak, J., et al. 2014, CEAB, 38, 53
Srivastava, A. K., Shetye, J., Murawski, K., et al. 2017, NatSR, 7, 43147
Stangalini, M. 2014, A&A, 561, L6
Stangalini, M., Consolini, G., Berrilli, F., De Michelis, P., & Tozzi, R. 2014, A&A, 569, A102
Stangalini, M., Giannattasio, F., Erdélyi, R., et al. 2017, ApJ, 840, 19
Stangalini, M., Giannattasio, F., & Jafarzadeh, S. 2015, A&A, 577, A17
Stein, R. F., & Nordlund, Å. 1998, ApJ, 499, 914
Stein, R. F., & Nordlund, Å. 2001, ApJ, 546, 585
Tomczyk, S., McIntosh, S. W., Keil, S. L., et al. 2007, Sci, 317, 1192
Tsuneta, S., Ichimoto, K., Katsukawa, Y., et al. 2008, SoPh, 249, 167
Viticchié, B., Del Moro, D., & Berrilli, F. 2006, ApJ, 652, 1734
Vögler, A., Shelyag, S., Schüssler, M., et al. 2005, A&A, 429, 335
Wang, H. 1988, SoPh, 116, 1
Yang, Y., Ji, K., Feng, S., et al. 2015a, ApJ, 810, 88
Yang, Y.-F., Qu, H.-X., Ji, K.-F., et al. 2015b, RAA, 15, 569
Yelles Chaouche, L., Moreno-Insertis, F., Martínez Pillet, V., et al. 2011, ApJL, 727, L30